IEEE Access
Multidisciplinary | Rapid Review | Open Access Journal

Received April 5, 2019, accepted April 24, 2019, date of publication April 29, 2019, date of current version May 7, 2019.

Digital Object Identifier 10.1109/ACCESS.2019.2913763

Breaking Overvoltage of Dry-Type Air-Core Shunt Reactors and Its Cumulative Effect on the Interturn Insulation

HONGYAN NIE[1,2], XIAOSHENG LIU[1], YONGHONG WANG[2], YUANHANG YAO[2], ZHEYI GU[2], AND CHAOHAI ZHANG[1]

[1]School of Electrical Engineering and Automation, Harbin Institute of Technology, Harbin 150001, China
[2]School of Electrical and Electronic Engineering, Harbin University of Science and Technology, Harbin 150080, China

Corresponding author: Hongyan Nie (niehongyan@hrbust.edu.cn)

This work was supported in part by the National Key Research and Development Program of China under Grant 2017YFB0902705, and in part by the China State Grid Corporation Science and Technology Project ''Research on Diagnostic Technology of High-Cold Operation of Substation Main Equipment''.

ABSTRACT The mechanism of overvoltage formation in the breaking process of a dry-type air-core shunt reactor (DTACSR) is studied in this paper. In addition, the effect of the overvoltage on the interturn insulation characteristics of the DTACSR is also discussed. Based on the actual working condition of a 66 kV DTACSR used in the Chinese power system, a three-phase simulation model and an equivalent circuit are proposed. The maximum chopping overvoltage and reignition overvoltage are obtained through the combination of theoretical analysis, simulation, and data fitting. An overvoltage accumulation test of the interturn insulation specimens is carried out with our established test platform, and the characteristic parameters of the interturn insulation specimens of the DTACSR in different stages of aging are measured. The results show that the combined method is very effective in evaluating the switching overvoltage of the DTACSR. Compared with the traditional single-phase circuit model, the proposed three-phase circuit model obtains a more accurate overvoltage equation. During the breaking process of a DTACSR, a chopping overvoltage with an amplitude greater than 5 p.u. and a reignition overvoltage with an amplitude greater than 8 p.u. may form. The cumulative effect of the overvoltage causes aging of the interturn insulation, and the degree of aging becomes more serious as the amplitude of the overvoltage increases.

INDEX TERMS Dry-type air-core shunt reactor, overvoltage, interturn insulation, cumulative effect.

I. INTRODUCTION

The dry-type air-core shunt reactor (DTACSR) has been widely used in reactive power regulation due to its comparative technical advantages [1]. As the number and service time of DTACSRs increase, the failure probability of a DTACSR increases [2], [3]. Related studies have demonstrated that the breakdown of interturn insulation has been identified as the main form of failure [4], [5]. A burning incident caused by interturn insulation faults would result in a large indirect economic loss [6]. Although several methods have been proposed for the detection of an interturn insulation fault [7], [8], the authors did not explain the origin of the interturn insulation fault. Overvoltages usually endanger the safe operation of interturn insulation and can cause an interturn insulation fault [9], [10]. The effect of overvoltage on the interturn insulation has been taken seriously. As a reactive power compensation device, a DTACSR is switched on frequently. Thus, switching overvoltages are the most frequent and harmful overvoltages impacting a DTACSR [11].

Many studies have contributed to the theoretical analysis of a single-phase circuit of an interrupting shunt reactor [12] and the simulation of the waveforms and amplitudes of overvoltages [13]. In addition, measurements of overvoltages and the corresponding current waveforms have been performed in the laboratory and on site [14], [15]. However, few works have focused on the theoretical analysis of three-phase circuits for switching a shunt reactor by a circuit breaker, the influence of related parameters on the waveforms of overvoltages, and the effect of overvoltages on the interturn insulation characteristics.

The associate editor coordinating the review of this manuscript and approving it for publication was Mehdi Bagheri.

To switch a reactor, a three-phase circuit breaker operates at the same time. In this paper, a 66 kV DTACSR and a SF_6 circuit breaker in a substation of the Northeast China Power Grid are taken as a prototype. A simulation model of the circuit breaker breaking a reactor in ATP-EMTP software and a three-phase equivalent circuit used for theoretical analysis are established. Theoretical analysis, a simulation and data fitting are used to determine the maximum chopping overvoltage and reignition overvoltage. The effect of the switching parameters on the overvoltage is considered. In addition, an experiment on the accumulative effect of overvoltages is carried out to measure the characteristic parameters for different aging periods. The mechanisms for the generation of overvoltages and the failure of the interturn insulation are discussed in this paper. These mechanisms are very helpful for improvements in the switching mode and the production engineering of a DTACSR.

II. SIMULATION ANALYSIS

A. THE STRUCTURE AND PARAMETERS OF A REACTOR

A DTACSR is mostly designed to have a multiencapsulation parallel structure, and each encapsulation contains multiple branches in parallel (see Fig. 1). Generally, the coils of a DTACSR are made of round aluminum wires with a diameter of 2 to 4 mm, and the round aluminum wires are surrounded by three layers of polyester film and one layer of nonwoven fabric. The materials used between two adjacent windings are composite insulation made of polyester film and nonwoven fabric impregnated with epoxy resin.

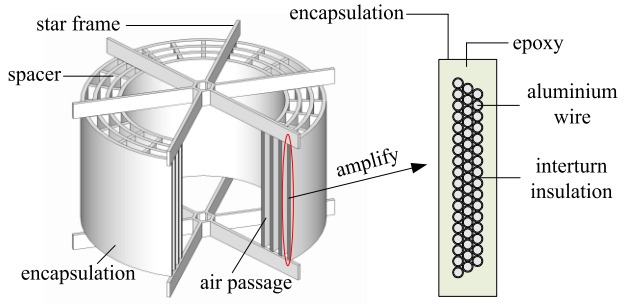

FIGURE 1. Structure of a dry-type air-core reactor.

The 66 kV DTACSR in the Northeast China Power Grid is selected as the object under study, and its main parameters are shown in Table 1.

B. SIMULATION MODEL

Each parameter is provided by the equipment manufacturer or estimated according to the actual size of the equipment.

1) BREAKER MODEL

The circuit breaker is an LTB72.5/D1 SF_6 circuit breaker, and its working characteristics mainly include the chopping current value, a high-frequency arc extinguishing ability and the medium recovery characteristics. The basic parameters of the circuit breaker are shown in Table 2.

TABLE 1. Parameters of the BKK-20000/66 DTASCR.

Rated voltage 38.11 kV	Rated capacity 20000 kVA	Rated frequency 50 Hz
Rated reactance 72.6 Ω	Inductance 231.2 mH	Winding resistance 0.217 Ω
Encapsulation 11	Encapsulation inner diameter (ID) 2.13 m	Encapsulation outer diameter (OD) 2.95 m
Minimum number of turns 351.85	Reactor height 3.18 m	Installation height 4.13 m

TABLE 2. Parameters of the circuit breaker.

Rated voltage	Breaking current	Closing speed	Opening speed
72.5 kV	40 kA	4.7 m/s	5.4 m/s

The current chop is caused by an arc instability. When the circuit breaker can suppress the arc discharge, the unstable arc plasma will be interrupted, and the current will be cut off before the zero-crossing. The current is usually called the current chop [16]. The chopping current is determined by the characteristics of the circuit breaker and the parameters of the external circuit. The value of the chopping current has a large dispersibility and is usually estimated as below.

$$i_{ch} = \lambda\sqrt{C_t} \tag{1}$$

where i_{ch} is the chopping current. λ is the chopping coefficient (namely, a circuit breaker characteristic that ranges from $4 \times 10^4 - 20 \times 10^4$ for a SF_6 puffer circuit breaker). C_t is the total capacitance of the external circuit and the circuit breaker in parallel [17], [18]. In [19], a SF_6 circuit breaker with a rated voltage of 300 kV was used to switch a 275 kV, 150 MVA reactor in the laboratory. The chopping current of the circuit breaker was detected to be between 0 and 30 A. As both the objects studied in this paper and in [19] are a SF_6 puffer circuit breaker, the chopping coefficient λ has the same range. Compared with the shunt reactor in [19], the voltage and capacity of the 66 kV, 20 MVA shunt reactor in this paper are much smaller, and the stray capacitance is much smaller. Therefore, the total capacitance C_t is small, and the chopping current is 0-13 A in this paper.

When the current frequency is greater than a limiting value, the circuit breaker can hardly extinguish the arc regardless of the other conditions. The limiting value of the current frequency is called the high-frequency extinguishing arc capability [20]. The high-frequency arc extinguishing capability of the LTB72.5/D1 SF_6 circuit breaker is between 50 and 300 A/μs, and its value is 100 A/μs in this paper.

When the circuit breaker is switched under no-load or light-load conditions, the change in the dielectric insulation strength between the contacts is an inherent characteristic of the circuit breaker, which is called the cold medium recovery characteristic [21]. The insulation strength between two contacts of the circuit breaker is closely related to the contact gap, the insulation medium, the gas pressure, and the

electric field distribution between the contacts [14]. In [22], the cold dielectric recovery characteristics of SF_6 gas during the switching of a 126 kV circuit breaker were studied, and a test circuit was built to measure the variation in the breakdown voltage with the contact gap of the circuit breaker. The gas pressure of the circuit breaker was 0.7 Mpa. The operating temperature was the ambient temperature. The fitting relationship between the breakdown voltage and the contact gap distance during the breaking process is defined as below.

$$\begin{cases} U_b = -0.02d^2 + 12d - 6.5 \\ d = 1000 \times vt \end{cases} \tag{2}$$

where U_b is the breakdown voltage, d is the contact opening distance, v is the contact opening speed, and t is time. In the test, $0 < d < 26$ mm. Substituting $d = 0$ into (2), $U_b = -6.5$ kV. Substituting $U_b = 0$ kV into (2), $d = 0.542$ mm. It is shown that when $0 < d < 0.542$ mm, there is a large error in the breakdown voltage calculated by (2). When the value of d is small, the amplitude of the reignition overvoltage is also small, so the influence of the calculation error on the maximum overvoltage can be ignored. The circuit breaker in this paper is different from the circuit breaker in [21] by one voltage level. However, the insulating medium is the same as SF_6, the gas pressure is 0.7 MPa, and the same electric field distribution between the contacts is used. Therefore, (2) can be used to represent the dielectric recovery characteristics of the LTB72.5/D1 SF_6 circuit breaker in this work. During the reignition of the circuit breaker, the breakdown time of the SF_6 gas between the contacts is a few nanoseconds, which is much smaller than the overvoltage settling time. After the SF_6 gas breaks down, the arc resistance is included in R_S (the busbar side damping resistance). Therefore, no specific arc model is used in the simulation.

According to the IEEE Std. C37.015-2009 guide for the application of DTACSR switching [23], the simulation model for the circuit breaker is shown in Fig. 2, where MODEL is a programmable control module and SW_TACS is a controllable switch. The closed switch SW_TACS is used when the circuit breaker is still closed or an arc occurs between the contacts of the circuit breaker. In contrast, when the arc between the two contacts is completely extinguished, the switch SW_TACS is open and two parallel branches are applied. One parallel branch consists of a resistance (R), a shunt inductance (L) and a shunt capacitance (C) in series, and the other branch is a resistance R_0. The shunt inductance (L) is 4 μH when the circuit breaker is open. The shunt capacitance (C) is the sum of the total stray capacitance including the contact dynamic capacitance when the circuit breaker is disconnected. Considering the influence of the shunt capacitance on the external circuit and the complexity of the contact capacitance, a fixed capacitance of 50 pF is used to represent the shunt capacitance (C) here. The resistance (R) is 10 Ω and is the oscillation loss resistance between L and C when the circuit breaker is reignited. The resistance (R_0) is 1 MΩ and is another oscillation loss resistance between L and $C$when the circuit breaker is opened.

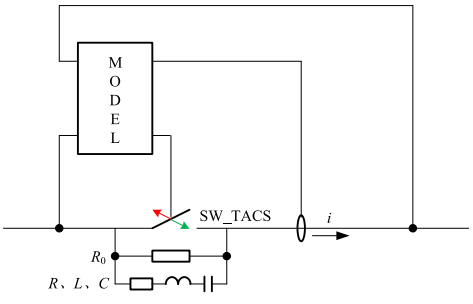

FIGURE 2. Simulation model of the circuit breaker.

According to the actual working characteristics of the circuit breaker during the breaking process of the DTACSR, the MODEL module is programmed. The specific values of the circuit breaker operating time (t_s), the chopping current (I_0), and the high-frequency arc extinguishing capability (f) are decided before the simulation. The initial state of SW_TACS is closed. The simulation time is ranged from 0 to 30 ms, and the time step is 10 ns. During the simulation, the MODEL module can automatically measure the power supply side voltage (U_1), the load side voltage (U_2) and the loop current (i), and it can also output the SW_TACS switch state. The working process of the MODEL module is shown in Fig. 3.

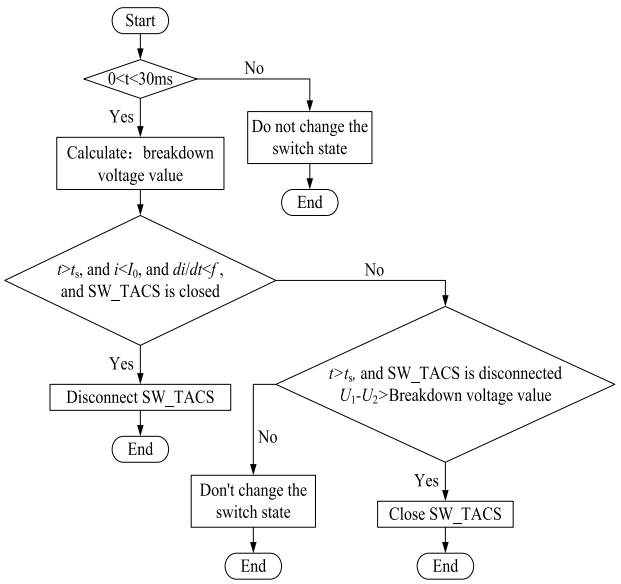

FIGURE 3. Workflow chart of the simulation model.

2) REACTOR MODEL

To investigate the overvoltage of the whole DTACSR, the equivalent lumped circuit of the DTACSR is used as shown in Fig. 4. L is the equivalent inductance, R_L is the equivalent resistance, C_Z is the equivalent capacitance, and C_{g1} and C_{g2} are the stray capacitances to the ground at both ends. These parameters as shown in Table 3 are estimated

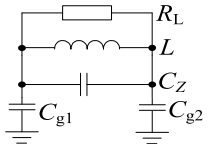

FIGURE 4. Equivalent lumped circuit for the overvoltage occurring in the DTACSR.

TABLE 3. Electrical parameters of the equivalent circuit.

L (mH)	R_L (kΩ)	Cz (pF)	Cg (pF)
231.2	330	100	118

according to the structural parameters and material properties of the studied BKK-20000/66 DTASCR.

3) SIMULATION CIRCUITS AND RESULTS

The connection mode of a 66 kV DTACSR in a power system is a three-phase star connection, and the neutral point is not grounded. According to the actual wiring, the simulation circuit model is established (see Fig. 5).

The other parameters in the simulation circuit are estimated according to the operating voltage and the length of the transmission line. These parameters include a busbar voltage of $V_S = 53.882$ kV, a busbar side line inductance of $L_S = 2$ mH, a busbar side equivalent capacitance of $C_S = 1$ μF, a busbar side damping resistance of $R_S = 10\,\Omega$, and an inductor between the circuit breaker and the reactor with an inductance of $L_W = 10$ μH.

In the simulation, it is assumed that the voltage equation of the A-phase DTACSR satisfies $U = 53.822 \times \cos \omega t$. When the phase angle is 180°, the voltage of the A-phase is a negative peak and the current crosses zero. As the grid frequency in China is 50 Hz, the zero-crossing point of the A-phase current is at 10 ms. The difference between the operating time of a circuit breaker and the time of the A-phase current zero is defined as the operating time lag (OTL). The random factors that affect the amplitude and type of overvoltages are mainly the OTL and the chopping current in the breaking process. For the 3-phase circuit, the OTL is ranged from 0 to 6.66 ms. When the OTL is greater than 6.66 ms, the overvoltage waveform of the A-phase DTACSR appears repeatedly on the B-phase DTACSR. In this study, the range of the chopping current is between 0 and 13 A. The three-phase currents successively pass through the zero point. These circuit breakers in the three-phase circuits will not be electrically disconnected at the same time. The phase in which the circuit breaker is electrically disconnected at the first time is defined as the first interrupting phase (FIP). The other two phases are defined as the last interrupting phase (LIP). Five typical overvoltage waveforms for each phase reactor are obtained via a simulation. Fig. 6 shows the overvoltage waveforms for the A-phase DTACSR. In Fig. 6, we can see that the oscillation frequency of the reignition overvoltage is much larger than that of the chopping overvoltage. In Fig. 6 (a) and Fig. 6 (b), the reignition occurs at the first current zero-crossing, and it is interrupted at the second current zero-crossing. In Fig. 6 (a), the reignition occurs when the chopping overvoltage does not reach its peak value. At the

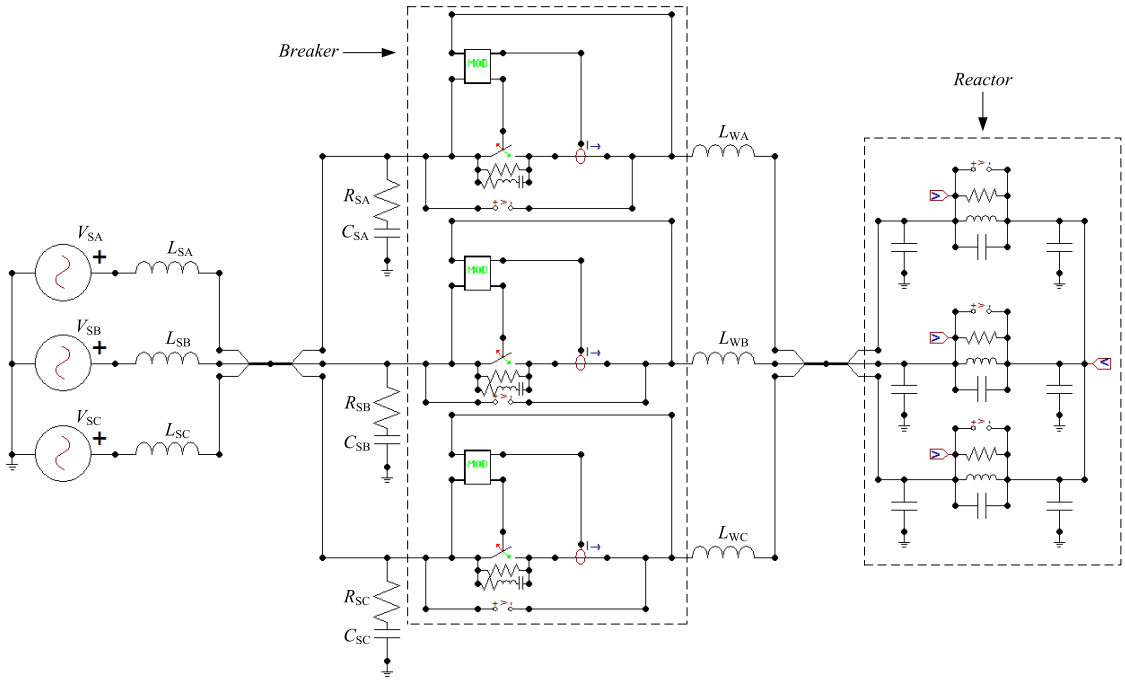

FIGURE 5. Simulation circuit.

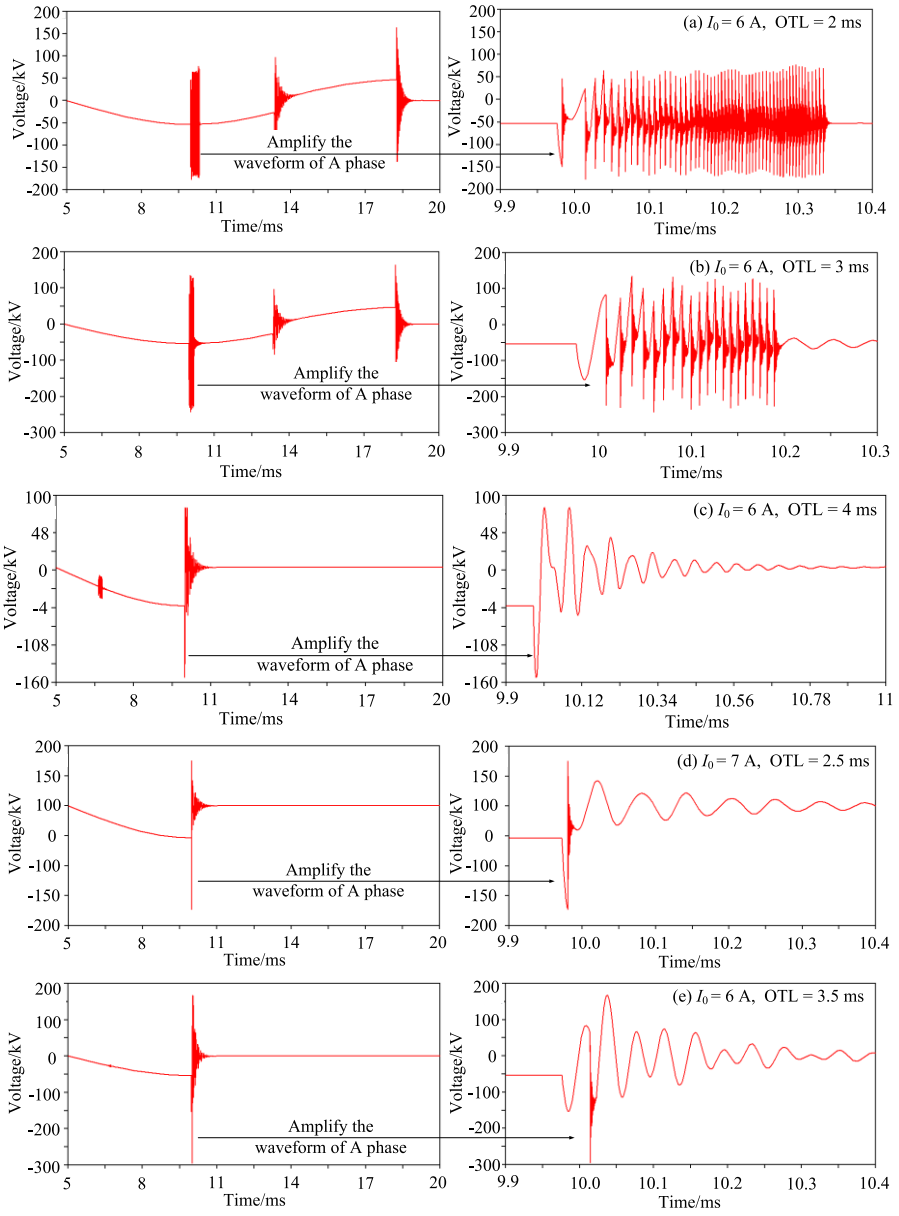

FIGURE 6. Typical overvoltage waveforms.

initial time of the reignition, the polarity of the end-to-ground voltage at the DTACSR is the same as that of the source-side voltage. At this time, $|U_b| = |U_g| - |U_0|$ is defined as the first type of reignition, where U_b is the breakdown voltage of the circuit breaker, U_g is the end-to-ground voltage, and U_0 is the busbar side voltage in the reignition phase. In Fig. 6 (b), the chopping overvoltage reaches the first peak and the reignition occurs during the reverse peak oscillation. At the initial moment of the reignition, the polarity of the end-to-ground voltage is opposite to that of the source-side voltage. At this time, $|U_b| = |U_g| + |U_0|$ is defined as the second type of reignition. In Figs. 6 (c), 6 (d), and 6 (e), the circuit breaker current can be cut off at the first zero-crossing of the A-phase current. Fig. 6 (c) shows that the reignition barely occurs, but multiple oscillations take place. Fig. 6 (d) shows that the first type of reignition occurs, whereas Fig. 6 (e) illustrates that the second type of reignition occurs.

The relationships between the overvoltage amplitude of the A-phase DTACSR and the chopping current for different OTLs are shown in Fig. 7. The variations in the overvoltage amplitude of the A-phase DTACSR against the OTL for different chopping currents are shown in Fig. 8.

In Fig. 7, the curves obtained with OTL = 3 ms (1 A $\leq$ I_0 $\leq$ 4 A), OTL = 4.5 ms (1 A $\leq$ I_0 $\leq$ 9 A), and OTL = 6 ms (1 A $\leq$ I_0 $\leq$ 13 A) correspond to the overvoltage waveform shown in Fig. 6 (c). This indicates that when no

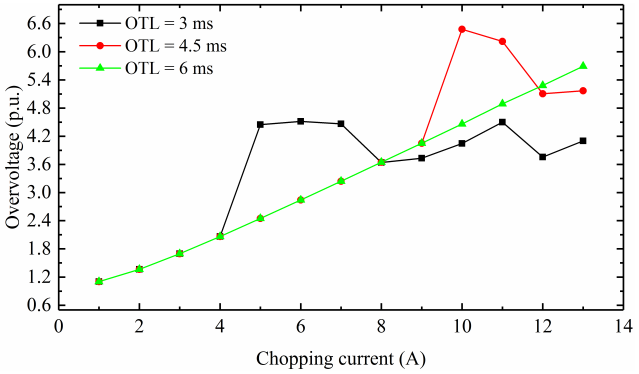

FIGURE 7. Relationships between the overvoltage amplitude and the chopping current.

reignition occurs, the chopping overvoltage increases with the chopping current. The curves obtained with OTL = 3 ms (5 A $\leq I_0 \leq$ 8 A) and OTL = 4.5 ms (10 A $\leq I_0 \leq$ 11 A) as shown in Fig. 7 correspond to the overvoltage waveform shown in Fig. 6 (b). In comparison, the curves obtained with OTL = 3 ms (9 A $\leq I_0 \leq$ 13 A and OTL = 4.5 ms (12 A $\leq I_0 \leq$ 13 A) as shown in Fig. 7 correspond to the overvoltage waveform shown in Fig. 6 (a). It can be seen that when the OTL is the same, the first type of reignition overvoltage (as shown in Fig. 6 (a)) with a larger chopping current is smaller in amplitude than the second type of reignition overvoltage (as shown in Fig. 6 (b)) with a smaller chopping current. For the same type of reignition overvoltage, when the OTL is different, the overvoltage with the larger chopping current is much larger in amplitude than that with a smaller chopping current. Thus, when the reignition occurs for the larger chopping current, the overvoltage is much larger in amplitude. Comparing the three curves in Fig. 7, we can observe that when the OTL is much larger, the current range for the occurrence of the reignition decreases. When OTL = 3 ms, the range of the chopping current for the occurrence of the reignition is 4-13 A. When OTL = 4.5 ms, this current range becomes 9-13 A, whereas no reignition occurs in the range of 0-13 A when OTL = 6 ms. Fig. 7 also shows that under the condition of OTL = 6 ms and I_0 = 13 A, the chopping overvoltage reaches a maximum value of 5.69 p.u.

Fig. 8 shows that, when the chopping current is constant, the A-phase DTACSR is shifted from the FIP (t = 10 ms, uncompleted chopping) into the LIP (t = 10 ms, completed chopping). The overvoltage waveforms corresponding to the curves of I_0 = 1 A (0.5 ms $\leq$ OTL $\leq$ 2 ms) and I_0 = 7 A (3 ms $\leq$ OTL $\leq$ 3.5 ms) are shown in Fig. 6 (b). The overvoltage waveforms corresponding to the curves of I_0 = 7 A (0.5 ms $\leq$ OTL $\leq$ 2 ms) and I_0 = 13 A (0.5 ms $\leq$ OTL $\leq$ 3.5 ms) are shown in Fig. 6 (a). The results show that, when the type of reignition is the same, the reignition overvoltage increases with increasing OTL. When the chopping current is much smaller, the reignition overvoltage occurring at the first current zero-crossing is a peak value. In contrast, when the chopping current is much larger, the A-phase DTACSR

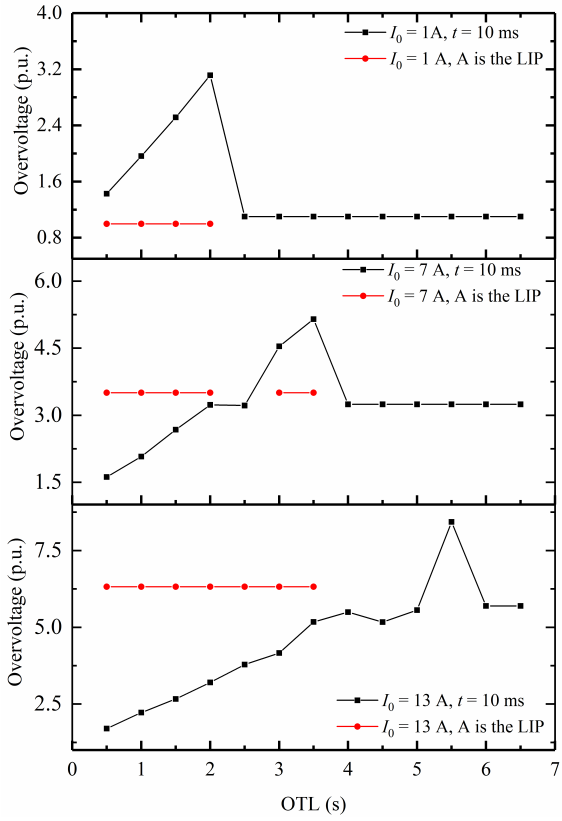

FIGURE 8. Relationships between the overvoltage and the OTL.

belongs to the LIP, and the chopping overvoltage occurring is a peak value. The curves as shown in Fig. 8 obtained for I_0 = 1 A (2.5 ms $\leq$ OTL $\leq$ 6.5 ms), I_0 = 7 A (4 ms $\leq$ OTL $\leq$ 6.5 ms), and I_0 = 13 A (6 ms $\leq$ OTL $\leq$ 6.5 ms) correspond to the waveforms shown in Fig. 6 (c). This indicates that the overvoltage amplitude is irrelevant to the OTL when no reignition occurs. Both curves shown in Fig. 8 obtained for I_0 = 7 A (2.5 ms $\leq$ OTL $\leq$ 3.5 ms) and I_0 = 13 A (4 ms $\leq$ OTL $\leq$ 6.5 ms) also show that the second type of reignition overvoltage is much larger in amplitude than the first type of reignition overvoltage when the chopping overvoltage is constant (i.e., the chopping currents are the same). The overvoltage waveforms corresponding to the curve of I_0 = 7 A (OTL = 2.5 ms) and the curve of I_0 = 13 A (4 ms $\leq$ OTL $\leq$ 5 ms) are illustrated in Fig. 6 (d). The overvoltage waveforms corresponding to the curve of I_0 = 13 A (OTL = 5.5 ms) are exhibited in Fig. 6 (e). These results show that in the breaking process of the DTACSR, reignition occurs at the first current zero-crossing point and is successfully interrupted. In addition, the overvoltage peak at this time is determined by the reignition overvoltage. Fig. 8 also shows that the larger the chopping current, the more complex the reignition type becomes. The maximum value of the reignition overvoltage is 8.43 p.u.

Based on the above analysis, the overvoltage in the breaking process of the DTACSR follows the rules stated below.

(A) When the chopping current is fixed, the overvoltage can be divided into three stages with increasing OTL. In the first stage, the reignition overvoltage occurs at the first current zero-crossing point, but the reignition is not interrupted. The overvoltage amplitude is the larger value of the reignition overvoltage at the first zero-crossing point and the overvoltage at the final cut-off. In the second stage, reignition occurs, it is successfully interrupted, and the overvoltage amplitude is the value of the reignition overvoltage. In the third stage, no reignition occurs, and the current is cut off at the first zero-crossing of the current. (B) When the OTL is constant, the chopping overvoltage increases in amplitude with increasing chopping current, and the current range for the occurrence of the reignition expands with the increase in the chopping current. (C) The larger the chopping overvoltage before the reignition occurs, the greater the amplitude of the reignition overvoltage becomes. (D) When the amplitude of the chopping overvoltage is equal before reignition, the second type of reignition overvoltage is much larger in amplitude than the first type of reignition overvoltage. Therefore, the maximum value of the overvoltage occurs at the largest chopping current for the second type of reignition. The first three rules are easy to understand. The reasons for the fourth rule are as follows. After disconnecting the current, reignition occurs when the difference between the end-to-ground voltage at the DTACSR and the busbar voltage reaches the breakdown condition of the circuit breaker. The end-to-ground voltage at the DTACSR is close to the bus voltage, and it oscillates with the bus voltage as the center and the breakdown voltage of the circuit breaker as the its amplitude. For the first type of reignition, the maximum value of the reignition overvoltage is $|U_0| + |U_b| - |U_n| = |U_g| - |U_n| = |U_{L0}|$ (where U_n is the neutral-point voltage, and U_{L0} is the chopping overvoltage of the initial reignition). For the second type of reignition, the maximum value of reignition overvoltage is $|U_0| + |U_b| - |U_n| = |U_g| - |U_n| + 2|U_0| = |U_{L0}| + 2|U_0|$.

III. THEORETICAL ANALYSIS

The theoretical equivalent circuit is shown in Fig. 9. In Fig. 9, V_S is the busbar voltage source, L_S is the busbar side lead inductance, C_S is the busbar side equivalent capacitance, R_S is the busbar side damping resistance, K is the circuit breaker switch, L_p is the equivalent inductance after breaking, C_p is the fracture capacitance after breaking, and L_w is the reactance-side lead inductor.

A. CHOPPING CURRENT OVERVOLTAGES

It is assumed that the A-phase is the FIP, whereas the B-phase and C-phase are the LIP. Three-phase reactors are coupled to each other. Compared with the parameters of the reactors, C_S is large enough, while R_S, L_p, and L_w are rather small. The high-frequency equivalent circuit for the A-phase is simplified as shown in Fig. 10 (a). When the A-phase DTACSR is disconnected, the neutral-point potential is offset. The B-phase and C-phase DTACSRs are connected in series to withstand the line voltage. The voltage applied to B-phase

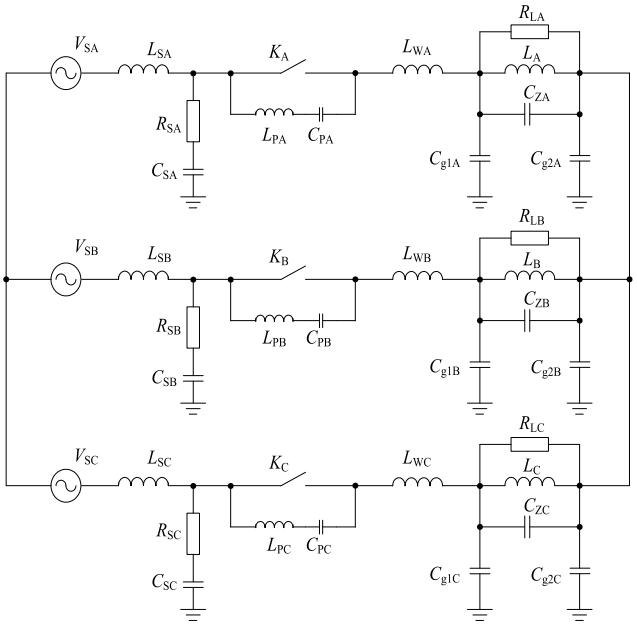

FIGURE 9. Theoretical equivalent circuit.

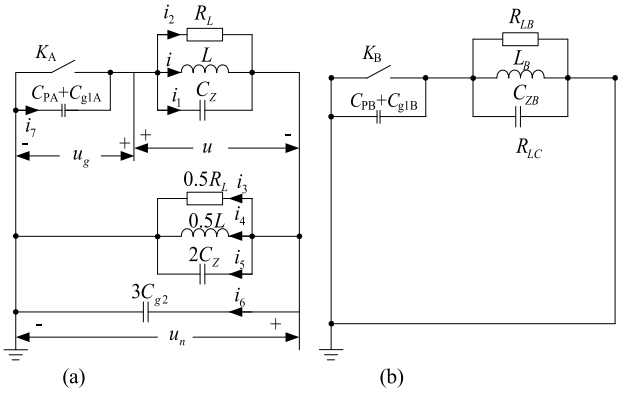

FIGURE 10. High-frequency equivalent circuits of chopping current overvoltages. (a) First interrupting phase. (b) Last interrupting phase.

or C-phase DTACSR is half of the line voltage. In addition, the neutral-point voltage jumping leads to the jumping of the voltage phase for the other two-phase DTACSRs. After a phase angle of 90°, for the other two-phase DTACSRs, the current crosses zero at the same time, and the voltage reaches the peak but has the opposite polarity. The peak value is $\sqrt{3}U_0/2$. When the LIP is open, since the parameters of the two-phase DTACSRs are the same, the high-frequency oscillation overvoltages of the two-phase DTACSRs have the same amplitude but opposite polarity, and the neutral-point voltage is zero. The high-frequency equivalent circuit of the chopping overvoltage applied to the two-phase DTACSR for the LIP is the same as the phase circuit, as shown in Fig. 10 (b).

In Fig. 10 (a), suppose that the voltage across the reactor is u, the end-to-ground voltage for reactor is u_g and the neutral-point-to-ground voltage is u_n. According to the relationships between the voltages and the currents of each

branch, the differential equation for voltage can be obtained as below.

$$\begin{cases} -L\left(C_p + C_{g1}\right)\dfrac{d^2u_g}{dt^2} = LC_Z\dfrac{d^2u}{dt^2} + L\dfrac{du}{R_L dt^2} + u \\ 1.5LC_{g2}\dfrac{d^2u}{dt^2} = L\left(C_Z + 1.5C_p + 1.5C_{g1} + 1.5C_{g2}\right) \\ \qquad \times\dfrac{d^2u_g}{dt^2} + L\dfrac{du_g}{R_L dt} + u_g \end{cases} \tag{3}$$

The fourth-order differential equations can be obtained by elimination, but they have no analytical solutions.

The voltage equation of the LIP reactors in Fig. 10 (b) is as follows.

$$L\left(C_Z + C_p + C_{g1}\right)\frac{d^2u}{dt^2} + L\frac{du}{R_L dt} + u = 0 \tag{4}$$

According to (4), the maximum value of the chopping overvoltage and the corresponding time can be obtained as below.

$$\begin{cases} t_0 = \dfrac{\arctan\left(\frac{\delta_1}{\omega_1}\right) + \varphi_1}{\omega_1} \approx -\dfrac{\varphi_1}{\omega_1} \\ u_{\max} = \exp\left(\dfrac{\delta_1\varphi_1}{\omega_1}\right)\sqrt{\dfrac{3}{4}U_0^2 + \dfrac{L}{C_Z + C_p + C_{g1}}I_2^0} \end{cases} \tag{5}$$

where $\omega_1 = \sqrt{\frac{1}{L(C_z+C_p+C_{g1})} - \delta_1^2}$ is the oscillatory angular frequency, $\delta_1 = \frac{1}{2R_L(C_z+C_p+C_{g1})}$ is the attenuation coefficient, $\varphi_1 = \arctan\frac{\sqrt{(L\times I_0)/(C_Z+C_p+C_{g1})}}{\sqrt{3}\,U_0/2}$ is the inception angle, and I_0 is the chopping current.

The analytical expression of the chopping overvoltage in the LIP can be obtained. However, the chopping overvoltage in the FIP cannot be obtained analytically. For the purpose of a practical engineering application, it is necessary to further study the expression of the chopping overvoltage in the FIP. The relationships between the maximum chopping overvoltage and different parameters are determined by a simulation. The expression of the overvoltages is obtained by data fitting.

Referring to the application guidelines for shunt reactors in IEEE Std. C37.015-2009, the possible ranges of the fracture capacitance parameters for the DTACSR and circuit breakers are shown in Table 4.

TABLE 4. Range of parameters.

Inductance	Ground stray capacitance	Longitudinal capacitance	Fracture capacitance
50-500 mH	50-250 pF	50-250 pF	50-250 pF

The chopping current $I_0 = 10$ A is used in the simulation. Based on (5) and the particular solutions of (3), a control variable method is used to fit the relationship between the maximum value of the chopping overvoltage and one parameter in Table 4. We finally obtain the following equation that contains four parameters for the maximum chopping overvoltages across the reactor in the FIP.

$$u_{\max} = \exp\left(\frac{\delta_2\varphi_2}{\omega_2}\right)\sqrt{U_0^2 + \frac{L}{K_c\left(C_Z + 1.5C_p + 1.5C_g\right)}I_0^2} \tag{6}$$

where $\omega_2 = \sqrt{\frac{1}{K_cL(C_Z+1.5C_p+1.5C_g)} - \delta_2^2}$ are the approximate oscillatory angular frequencies, $\delta_2 = \frac{1}{2R_LK_c(C_Z+1.5C_p+1.5C_g)}$ are the approximate attenuation coefficients, and $\varphi_2 = \arctan\frac{\sqrt{(L\times I_0)/[K_c\times(C_Z+1.5C_p+1.5C_{g1})]}}{U_0}$ is the inception angle. K_c is a correction factor for the capacitance and can be described as follows.

$$K_c = 1.15\left(0.934 + 0.0869L\right) \times\left[0.896 - 1.56\times10^8\left(3C_g - C_Z - C_p\right)\right]$$

B. REIGNITION OVERVOLTAGES

When the chopping overvoltage of the reignition phase reaches a maximum value, the reignition overvoltage will reach a maximum value. Since the oscillation frequency of the reignition overvoltage is very high, the self-inductance and self-resistance of the DTACSR can be neglected. In other words, the energy is mainly converted between the lead inductor and the equivalent capacitances that consist of the interturn capacitance and the stray capacitance to the ground of the three-phase DTACSR.

The reignition causes the reactor to be connected to the power system again. As the neutral point is not grounded, the oscillating overvoltages are also produced within the reactor. The inductance of the reactor is much larger than the lead inductance in the oscillation circuit, so the internal oscillation frequency is much lower than the reignition oscillation frequency. The effect of an internal oscillation on the reignition overvoltage can be neglected when the maximum value of the reignition overvoltage at the initial time of reignition is analyzed. After a single reignition, once the condition is satisfied, reignition will occur again, and multiple reignitions occur during the breaking process.

We need to know the initial values of the voltage across the reactor and the end-to-ground voltage to calculate the reignition overvoltage. Due to the multiple oscillations in the circuit, the initial value cannot be obtained by extending time as in the method used for (6). Therefore, based on (6), the equation of the reignition overvoltage is obtained below by the same method as that in Section III A.

$$u_{\max} = \exp\left(\delta_2\frac{\pi + \varphi_2}{\omega_2}\right) \times\sqrt{K_{fi}U_0^2 + K_{fi}\frac{L}{K_u\left(C_z + 1.5C_p + 1.5C_g\right)}I_0^2} \tag{7}$$

where K_{fu} is the voltage correction coefficient, and K_{fi} is the current correction coefficient. Their equations are described

as follows.

$$K_{fu} = 7.87 \times \left(-0.23\,L^2 + 0.122\,L + 0.486\right) \times \left(-4.89 - 0.234 \ln C_g\right) \times \left(6.93 + 0.279 \ln C_z\right) \times \left(3.67 \times 10^{18} C_p^2 - 8.01 \times 10^8 C_p + 0.535\right)$$

$$K_{fi} = 297 \times \left(0.37\,L^2 - 0.392\,L + 0.216\right) \times \left(9.68 \times 10^{18} C_g^2 - 4.36 \times 10^9 C_z + 0.501\right) \times \left(-3.43 \times 10^{18} C_z^2 + 1.36 \times 10^9 C_z^2 + 1.89 \times 10^9 C_z - 0.116\right) \times \left(9.01 \times 10^{18} C_p^2 - 1.46 \times 10^9 C_p + 0.191\right)$$

As the three-phase circuit operates in a neutral non-grounded manner, the neutral-side stray capacitance to ground of the three-phase DTACSR can affect the overvoltage generation. The stray capacitance to the ground (C_g) is taken into account in (5), (6), and (7). This indicates that, compared with the single-phase circuit model, the proposed three-phase circuit model is much closer to the actual operating condition and can obtain more accurate results.

C. DISCUSSION

1) ANALYSIS OF THE EFFECTIVENESS OF THE SIMULATION RESULTS

When reignition does not occur, the chopping overvoltage is constant and has a maximum value. Its per-unit value is 1 p.u. $= U_0 =$ 53.882 kV. The relationships among the simulated value of the maximum overvoltage in the first and last phase, the calculated values obtained by (5) and (6), and the chopping current are shown in Fig. 11.

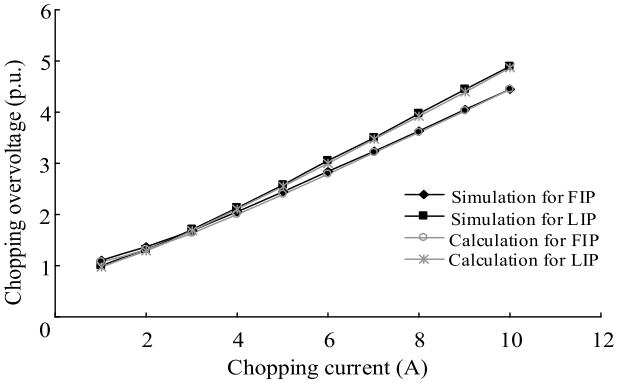

FIGURE 11. Relationship between the maximum chopping overvoltage and the chopping current.

As can be seen from Fig. 11, the simulated values are in good agreement with the calculated values. (5) is the analytical solution, so the curve drawn by the calculated value of the maximum chopping overvoltage for the LIP can be used as a reference. The simulated value of the maximum chopping overvoltage for the LIP is consistent with the calculated value, which proves that the simulation results are reliable. The simulated value of the maximum chopping overvoltage for the FIP is consistent with the calculated value, which proves that it is reasonable to use (7) to estimate the maximum chopping overvoltage. When the chopping current is 10 A, the maximum overvoltage is more than 5 p.u.

A series of simulated values for the maximum reignition overvoltage is obtained by adjusting the OTL. The relationships between the calculated values and the simulation results according to (7) are shown in Fig. 12. The simulated values are in good agreement with the calculated values in Fig. 12. When the chopping current is 10 A, the maximum reignition overvoltage is more than 7 p.u.

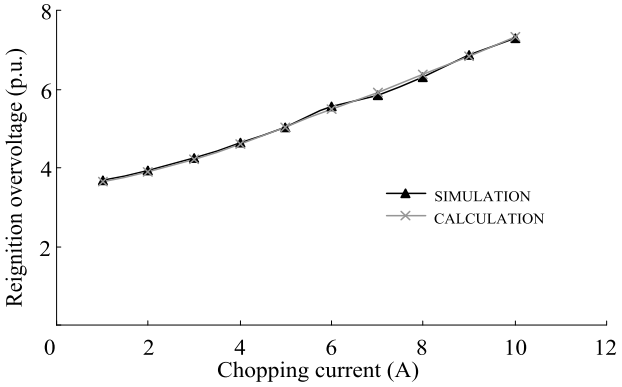

FIGURE 12. Relationship between the maximum reignition overvoltage and the chopping current.

2) ACCURACY OF THE THREE-PHASE ANALYSIS MODEL OF OVERVOLTAGE

The single-phase analysis circuit of the circuit breaker breaking a shunt reactor recommended in IEEE Std C37.015-2009 is shown in Fig. 13 (a). The high-frequency equivalent circuit is shown in Fig. 13 (b) when the circuit breaker is disconnected.

In Fig. 13, C_L is the total capacitance to the ground of the single-phase reactor and consists of the interturn capacitance C_Z and the head-to-ground capacitance C_{g1}. The other parameters are consistent with those in the three-phase circuit.

Comparing Fig. 13 (b) with Fig. 10 (a), as the neutral point of the single-phase circuit is directly grounded, the single-phase circuit does not consider the influences of the other two-phase reactor parameters and the stray capacitance to the ground of the neutral point. Moreover, the capacitance equivalent to the neutral-point side of the reactor cannot be negligible compared with the interturn capacitance of the reactor and the fracture capacitance of the circuit breaker. Furthermore, the single-phase circuit cannot be used to analyze the overvoltage condition for the LIP. Therefore, the analysis results of the three-phase circuit have much higher accuracy than those of the single-phase circuit.

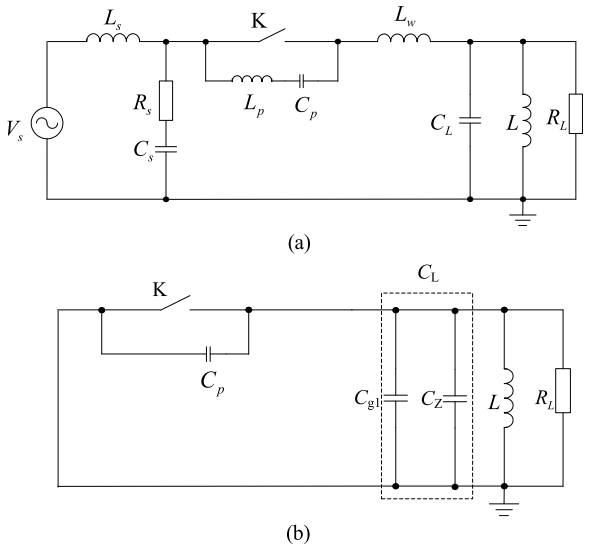

FIGURE 13. Single-phase circuit of the circuit breaker breaking a shunt reactor and its high-frequency equivalent circuit. (a) Single-phase analysis circuit. (b) High-frequency equivalent circuit.

IV. THE EFFECT OF THE BREAKING OVERVOLTAGE ON THE INTERTURN INSULATION CHARACTERISTICS

The DTACSR is a parallel structure of multibranch coils with many turns. Due to a large number of coil turns and the whole curing method, local insulation defects are inevitably located in the DTACSR. In addition, the local interturn insulation defects may be caused by electrical stress during the operation of the DTACSR. Under the application of a high electric field, partial discharge (PD) usually occurs in the defect location at first. Repeated PDs can cause cumulative damage to the solid insulation and even lead to the breakdown of the insulation materials. Therefore, it is necessary to study the cumulative effect of the breaking overvoltage on the interturn insulation properties of the DTACSR.

A. INTRODUCTION TO THE EXPERIMENT

1) MODEL SPECIMEN AND ELECTRODE

When the actual DTACSR operates, the potentials of the aluminum wires at the same height in different branches are almost equal. The electric field only exists between the upper and lower adjacent turns and can be considered as an electric field between two typical infinitely long parallel cylinders. The polyester-film-coated aluminum wire used in the actual DTACSR is selected as the object under study. The diameter of the bare aluminum wire is 4 mm and the diameter of the insulating coated aluminum wire is 4.4 mm. A segment of the insulating coated aluminum wire with a length of 300 mm is used. The ends are curved, and the length of the middle parallel section that is used to simulate the interturn insulation of the DTACSR is 140 mm. Thus, the formed electric field can be regarded as the electric field of infinitely long parallel cylinders.

The middle part of the two aluminum wires is parallel, and their end insulation is removed. In the bifurcation position of samples, the polyimide film is twined by semilapping to strengthen the insulation, and a nylon band is used to lock wires. Referring to the proportion scheme provided by the reactor manufacturer, epoxy resin is used to solidify samples. The epoxy resin is fully stirred and placed at 60°C for 1 h. After pretreatment, the epoxy resin is painted on the surface of the specimens. The specimens coated with epoxy resin are put into a thermostat at a constant temperature of 80°C for 4 h and then naturally cooled for 24 h. The specimen is installed in the electrode in Fig. 14.

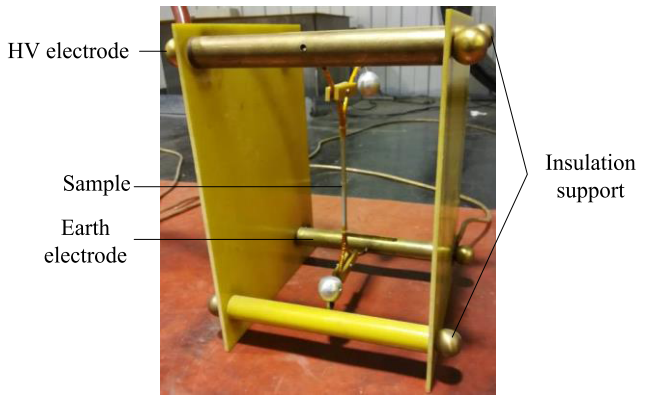

FIGURE 14. Specimens and electrode system.

2) TEST DEVICES

To study the influence of the breaking overvoltage on the interturn insulation performance, a device to generate an exponentially decaying oscillating voltage was designed and constructed with IEC Std. 60076-6 as a reference. The principle circuit of the test device is shown in Fig. 15. The power supply of the test device supplies 220 V at 50 Hz. The AC high voltage is obtained by the voltage regulator T_1 and the power frequency testing transformer T_2. During the negative half cycle of the power frequency voltage, the high-voltage silicon stack D is turned on, and the main capacitor C_C is charged. At the zero-crossing of the power supply frequency from negative to positive, the high-voltage silicon reactor D is turned off. The trigger signal is sent by the control circuit and is amplified by the pulse transformer T_3 to generate the pulse voltage. This pulse voltage is applied to the "needle-skin" of

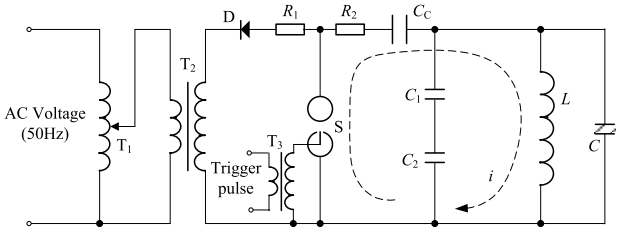

FIGURE 15. The test circuit of the interturn overvoltage.

the sphere gap S to generate a small arc, inducing the main gap of the sphere gap S to turn on. The energy stored in the main capacitor is discharged through the damping resistor R_2 to the inductor L and the specimen C.

Since the equivalent capacitance C of the specimen is small, it can be ignored in parallel with the inductance L. Assume that the total resistance in the discharge circuit of the main capacitor to the inductor coil and the model specimen is R, the initial charging voltage of the main capacitor is U_{C0}, and the initial current of the inductor coil is 0. Then, the discharge loop can be equivalent to Fig. 16.

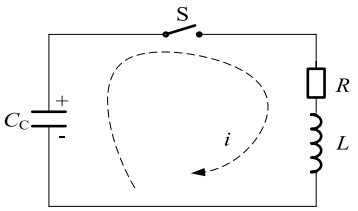

FIGURE 16. The discharge circuit.

The switch is turned on at $t = 0$. The voltage and current equations of the loop can be solved, and the equations of the loop current i and the voltage of the inductor can be obtained as shown below.

$$i = -\frac{1}{\omega L} U_{C0} e^{-\hat{\alpha}} \sin(\omega t) \tag{8}$$

$$U_L = \frac{\omega_0}{\omega} U_{C0} e^{-\hat{\alpha}} \sin(\omega t - \beta) \tag{9}$$

where $\omega_0 = 1/\sqrt{LC_C}$ is the natural oscillated frequency, $\delta = R/(2L)$ is the attenuation coefficient, $\omega = \sqrt{\omega_0^2 - \delta^2}$ is the virtual oscillated frequency, and $\beta = \arctan(\omega/\delta)$ is the initial phase.

It can be seen from (9) that the voltage applied to the model specimen is an exponentially decaying oscillating wave.

The number of discharges of the test device is determined by the trigger control signal. The control circuit sends a trigger signal in each power frequency power cycle, and the time relay installed in the control circuit can work continuously for one minute at a time. Therefore, the device used to generate an exponentially decaying oscillating voltage can output 3,000 exponentially decaying oscillating waves in one minute. That is, one charge and discharge process takes 20 ms. The high-voltage part of the test device is structured as shown in Fig. 17. The high-voltage silicon reactor, the protection resistor, and the power frequency test transformer in the principle circuit are integrated in the DC high-voltage generator.

The voltage waveform on the specimen is measured by an oscilloscope connected to a voltage divider consisting of C_1 and C_2 (the voltage division ratio is 1000/1). The waveform of a one-time overvoltage acquired by the oscilloscope is shown in Fig. 18. From Fig. 18, the duration of the one-time overvoltage is 0.5 ms, so the time interval between two succession overvoltage pulses is 19.5 ms.

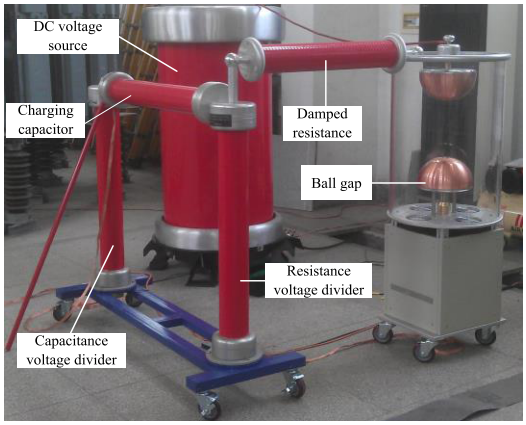

FIGURE 17. Device used to generate an exponentially decaying oscillating voltage.

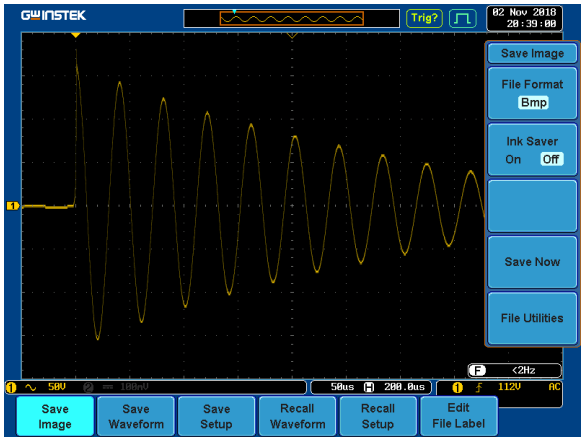

FIGURE 18. Waveform of a one-time exponentially decaying oscillating voltage.

A PD test system is built in a shielded room. The PD detector is Hipotronics DDX-7000 with a sampling frequency of 80 MHz and a sensitivity of 0.1 pC. Before the PD test is formally carried out, the voltage of the test system is increased to 5 kV under the condition that the electrode system is not connected to the sample, at which time the discharge of the test system is less than 5 pC. When the PD signal is measured formally, the voltage increases slowly from 0 V, and the pulse signal is detected on the detector. When the voltage increases to a certain value, if the discharge is more than 5 pC and repeats in a given time period, the voltage value is recorded as the PD initial voltage (PDIV) and the characteristic parameters of the PD are collected by the DDX-DA3 advanced analysis module inside the detector.

3) TEST SCHEME

Before the formal test, 12 samples are subjected to the breakdown test with the exponentially decaying oscillation voltage. The maximum and minimum values are eliminated, and the mean breakdown voltage and standard deviation are 35.59 and 1.79 kV, respectively. The branch with the fewest

turns of the reactors studied has 351.85 coil turns, and the average power frequency potential between turns is 153 V. Considering the switching process occurs in extreme weather such as rain, snow and fog, the damp and the uneven voltage distribution of the local interturn insulation could be caused by the local moisture on the outer surface of the DTACSR. This leads to an increase in the overvoltage amplitude in partial interturn insulation. Based on the validity of the data and the test cycle, five voltages of 10, 12, 14, 16, and 18 kV are selected as test voltages for the cumulative damage, and 10 valid data points are taken for 12 specimens at each voltage. To obtain the PD characteristics of the specimens in the early stage of aging, the number of cumulative overvoltages is taken to be 3,000, 15,000, 30,000, 60,000, and 90,000. The insulation resistance (IR) and PD parameters of the specimens are measured at the end of each test cycle. The PD parameters include the PD inception voltage, the PD maximum magnitude, and the discharge power. After all aging cycles are completed, five specimens are selected randomly for the breakdown test with an exponentially decaying oscillating voltage for each aging voltage, and the remaining five specimens are subjected to a power frequency breakdown test.

B. TEST RESULTS AND ANALYSIS

The variation curves of the characteristic parameters under an exponentially damped oscillation overvoltage are shown in Fig. 19.

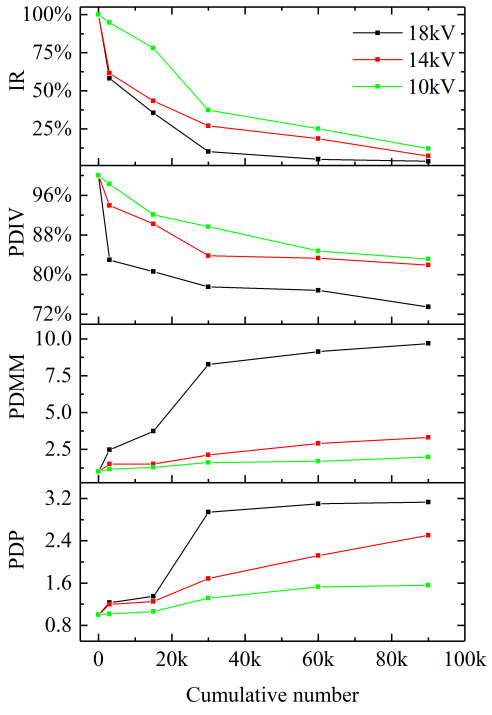

FIGURE 19. The relationship between the characteristic parameters and number of cumulative overvoltages.

Each data point is the average of 10 test data points. The IR and the PDIV decrease with the cumulative numbers. The PD maximum magnitude (PDMM) and the PD power (PDP) increase with the cumulative numbers. To eliminate the interference of the specimen preparation process and the test environment on the test results, the IR and PDIV after aging are denoted by the percentage of their values before aging, whereas the PDMM and PDP after aging are denoted by the multiples of their values before aging. From Fig. 19, taking the samples with the voltage of 14 kV as an example, when the number of cumulative overvoltages is 3,000, 15,000, 30,000, 60,000, and 90,000, respectively, the IR decreases to 61.5 %, 43.3 %, 27.0 %, 18.6 %, and 7.2 % of the initial values; the PDIV decreases to 93.9 %, 90.2 %, 83.8 %, 83.3 %, and 81.9 % of the initial values; the PDMM increases by factors of 1.55, 1.51, 2.12, 2.90, and 3.31; and the PDP increases by factors of 1.20, 1.25, 1.69, 2.12, and 2.50. The samples with the voltage of 10 kV and 18 kV exhibit similar dependences.

For the voltages of 10, 12, 14, 16, and 18 kV, when the number of cumulative overvoltages is 90,000, compared with the breakdown voltage of unaged samples, the power frequency breakdown voltage decreases to 97.4 %, 96.32 %, 93.8 %, 91.9 %, 88.5 %, respectively. The exponentially decaying oscillating breakdown voltage decreases to 97.6 %, 96.45 %, 94.1 %, 92.08 %, and 88.73 % of the unaged breakdown voltage, respectively. The relationship between the average value of the breakdown voltage and the aging voltage is shown in Fig. 20.

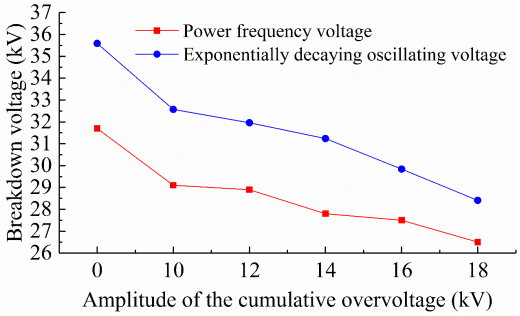

FIGURE 20. Breakdown voltage at the power frequency and with the exponentially decaying oscillating voltage.

As seen from Fig. 19, the range of the variation in each characteristic parameter is large in the initial stage of the accumulation, and the variation decreases in the later stage. From Fig. 20, when the cumulative overvoltages reach a certain value, that is, the electrical aging reaches a certain level, the breakdown voltage of the specimen decreases for the five aging voltage levels. This indicates that the electrical aging will affect the breakdown voltage of the DTACSR. It can also be seen from Fig. 20 that the average value of the breakdown voltage of the model specimens monotonously decreases with the increase in the cumulative overvoltage amplitude.

According to the variation in the characteristic parameters with the cumulative overvoltages, the mechanism of damage

of the interturn insulation is analyzed for an exponentially decaying oscillation overvoltage. During the manufacturing process, air gap defects can be produced in the interturn insulation. The electric field distribution with an oscillation voltage is inversely proportional to the relative permittivity (φ). Thus, the electric field in the air gap is approximately three times stronger than that in the solid insulation ($\varphi_{\mathrm{PET}} \approx 3$, $\varphi_{\mathrm{air}} \approx 1$). According to the PDIV, PD occurs in the sample when the voltage is close to 3.5 kV. Therefore, the PD is caused by the breakdown of air gap defects due to the overvoltage. The molecular bonds of organic materials around the air gaps breakdown into molecules with a lower molecular weight under the impact of high-energy charged particles. The short-term high temperature produced by PD causes a partial carbonization of organic insulating materials. Highly active H•, O•, and HO• lead to chemical degradation of organic materials and corrosion of the surrounding insulation materials, resulting in impurity carriers. All these factors will gradually result in a reduction of the insulation properties of the material. As the aging process increases, the discharge will develop from the edge of the air gap to the interior of the solid insulating material, leading to an expansion of the air gap and an increase in the discharge channel. As the cumulative effect increases, the IR that can characterize the macroinsulation properties of the samples decreases. The PDIV used to represent the minimum insulation defect may decrease. The PDMM characterizing the largest insulation defect increases. The PDP, which includes the pulse discharge, pulse count, and instantaneous value of the voltage, reflects the aging process and can increase with aging. The cumulative effect of the overvoltage causes the breakdown voltage of the model specimen to decrease. The aging voltage value is larger, and the breakdown voltage decreases faster.

V. CONCLUSION

The mechanism of overvoltage formation is studied when a DTACSR is switched off. Moreover, the influence of the switching overvoltage on the interturn insulation characteristics of the DTACSR is also investigated. Several main conclusions are drawn as below.

(1) The combination of theoretical analysis, simulation, and data fitting are used to estimate the equation of the reignition overvoltage and chopping overvoltage generated in the process of a circuit breaker switching off the DTACSR.

(2) Compared with the single-phase circuit model, a more accurate overvoltage equation is obtained with the proposed three-phase circuit model.

(3) The random factors affecting the amplitude of the overvoltage during the breaking process mainly include the chopping current and the OTL. A stronger chopping current results in a higher overvoltage and a larger reignition area. If arc reignition occurs, the amplitude of the overvoltages will be larger. The OTL has little effect on the chopping overvoltage, but it can affect the occurrence and types of reignition and the amplitude of the reignition voltage.

(4) When a 66 kV DTACSR is switched off by a circuit breaker, the chopping overvoltage may be greater than 5 p.u. in amplitude, and the reignition overvoltage may be greater than 8 p.u. in amplitude.

(5) The cumulative effect of the exponentially decaying oscillation overvoltage can cause irreversible damage to the interturn insulation of the DTACSR as the reactors are switched off. Compared with the unaged samples, the IR and PDIV decrease by 6.71 % and 73.461 % of the initial values, respectively. The PDMM and PDP increase to 9.86 times and 3.17 times the initial values, respectively. The power frequency and exponentially decaying oscillating voltage decrease to 88.5 % and 88.73 % of the initial values, respectively.

REFERENCES

[1] M. Enohnyaket and J. Ekman, "Analysis of air-core reactors from DC to very high frequencies using PEEC models," *IEEE Trans. Power Del.*, vol. 24, no. 2, pp. 719–729, Apr. 2009.

[2] M. Nagpal, T. G. Martinich, A. Bimbhra, and D. Sydor, "Damaging open-phase overvoltage disturbance on a shunt-compensated 500-kV line initiated by unintended trip," *IEEE Trans. Power Del.*, vol. 30, no. 1, pp. 412–419, Feb. 2015.

[3] A. A. Dahab, P. E. Burke, and T. H. Fawzi, "A complete model of a single layer air-cored reactor for impulse voltage distribution," *IEEE Trans. Power Del.*, vol. 3, no. 4, pp. 1745–1753, Oct. 1988.

[4] H. Nie, J. Liang, Y. Wang, C. H. Zhang, and X. S. Liu, "Research on pulse oscillating circuit of turn-to-turn over-voltage test for reactors," in *Proc. IEEE Int. Conf. Electr. Power Equip. Switching Technol.*, Matsue, Japan, Oct. 2013, pp. 1–4.

[5] *Power Transformers—Part 6: Reactors*, IEC Standard 60076-6, 2013.

[6] S. Das, T. S. Sidhu, M. R. D. Zadeh, and Z. Zhang, "A novel hybrid differential algorithm for turn to turn fault detection in shunt reactors," *IEEE Trans. Power Del.*, vol. 32, no. 6, pp. 2537–2545, Dec. 2017.

[7] *Requirements, Terminology, and Test Code for Dry-Type Air-Core Series-Connected Reactors*, IEEE Standard C57.16 TM, 2011.

[8] L. Zhang *et al.*, "Field test on the turn-to-turn insulation for 35 kV dry-type air-core reactors," *Electr. Mach. Control*, vol. 18, no. 6, pp. 66–71, Nov. 2014.

[9] G. Mazzanti and G. C. Montanari, "Electrical aging and life models: The role of space charge," *IEEE Trans. Dielectrics Electr. Insul.*, vol. 12, no. 5, pp. 876–890, Oct. 2005.

[10] L.-J. Yang, S.-H. Gao, B.-F. Deng, J. Tang, and J.-J. Huang, "Effects of electric fields on copper sulfide deposition and the properties of insulating oils in oil-immersed transformers," *IEEE Trans. Dielectr. Electr. Insul.*, vol. 24, no. 5, pp. 2847–2853, Oct. 2017.

[11] Q. Xie, J. Ren, H. Huang, K. Fu, C. Zhang, and T. Shao, "Aging characteristics of epoxy resin discharged by very fast transient overvoltage in SF_6," *IEEE Trans. Dielectr. Electr. Insul.*, vol. 24, no. 2, pp. 1178–1188, Apr. 2017.

[12] Y. An, X. Wen, T. Zhang, K. Ma, Y. Wang, and X. Chen, "Overvoltage of shunt reactor caused by prebreakdown of SF_6 breaker and protection measures," *High. Voltage Eng.*, vol. 39, no. 1, pp. 75–80, Jan. 2013.

[13] Z. Ma, C. A. Bliss, A. R. Penfold, A. F. W. Harris, and S. B. Tennakoon, "An investigation of transient overvoltage generation when switching high voltage shunt reactors by SF_6 circuit breaker," *IEEE Trans. Power Del.*, vol. 13, no. 2, pp. 472–479, Apr. 1998.

[14] D. F. Peelo and E. M. Ruoss, "A new IEEE application guide for shunt reactor switching," *IEEE Trans. Power Del.*, vol. 11, no. 2, pp. 881–887, Apr. 1996.

[15] N. Du, Y. Guan, J. Zhang, J. Niu, S. Yao, and G. Xu, "Phenomena and mechanism analysis on overvoltages caused by 40.5-kV vacuum circuit breakers switching off shunt reactors," *IEEE Trans. Power Del.*, vol. 26, no. 4, pp. 2102–2110, Oct. 2011.

[16] G. W. Chang, H. M. Huang, and J.-H. Lai, "Modeling SF_6 circuit breaker for characterizing shunt reactor switching transients," *IEEE Trans. Power Del.*, vol. 22, no. 3, pp. 1533–1540, Jul. 2007.

[17] *High-Voltage Switchgear and Controlgear—Part 110: Inductive Load Switching*, IEC Standard 62271-110, 2017.

[18] G. W. Chang, H. M. Huang, and J.-H. Lai, "Modeling SF_6 circuit breaker for characterizing shunt reactor switching transients," in *Proc. Int. Conf. Power Syst. Technol.*, Singapore, 2004, pp. 1315–1320.
[19] H. Kawada *et al.*, "Switching surge of shunt reactor caused by sf6 circuit breaker operation," *IEEE Trans. Power Del.*, vol. 2, no. 4, pp. 1124–1130, Oct. 1987.
[20] S. Okabe, M. Kosakada, H. Toda, K. Suzuki, and M. Ishikawa, "Investigations of multiple reignition phenomena and protection scheme of shunt reactor current interruption in GIS substations," *IEEE Trans. Power Del.*, vol. 8, no. 1, pp. 197–202, Jan. 1993.
[21] F. Wang, B. Zhang, Y. Tian, F. Lang, X. Lin, and Y. Xia, "Test analysis of dielectric recovery characteristic in high voltage SF_6 circuit breaker," in *Proc. Int. Conf. Electr. Equip.-Switching Technol.*, Xi'an, China, Oct. 2017, pp. 11–15.
[22] X. Lin, F. Wang, W. Liu, Y. Xia, J. Xu, and J. Zhong, "Experiment researches on cold state dielectric recovery characteristics in high voltage SF_6 circuit breakers," (in Chinese), *Proc. CSEE*, vol. 36, no. 14, pp. 3973–3981, 2016.
[23] *IEEE Guide for the Application of Shunt Reactor Switching*, IEEE Standard C37.015 TM, 2009.

HONGYAN NIE received the B.S. and M.S. degrees in electrical engineering from the Harbin University of Science and Technology, Harbin, China, in 2007 and 2010, respectively. He is currently pursuing the Ph.D. degree with the Harbin Institute of Technology, Harbin. He is also an Associate Professor with the School of Electrical and Electronic Engineering, Harbin University of Science and Technology. His research interests include insulation structure design, insulation diagnosis, and high voltage test technology of power equipment.

XIAOSHENG LIU received the B.S. and M.S. degrees in electrical engineering from the Harbin Institute of Technology, Harbin, China, in 1988 and 1993, respectively, where he is currently a Professor with the Department of Electrical Engineering. His research interests include smart grid communication, building electrical intelligence, and wireless energy transmission and the energy Internet.

YONGHONG WANG was born in Hebei, China, in 1972. He received the M.Sc. and Ph.D. degrees in electrical engineering from the Harbin University of Science and Technology, where he is currently a Professor. His major research fields are high voltage test technology and online monitoring of electric equipment.

YUANHANG YAO received the B.S. and M.S. degrees in electrical engineering from the Harbin University of Science and Technology, Harbin, China, in 2014 and 2017, respectively, where he is currently a Lecturer with the School of Electrical and Electronic Engineering. His research interests include insulation testing and high voltage testing technology of power equipment.

ZHEYI GU received the B.S. and M.S. degrees in electrical engineering from the Harbin University of Science and Technology, Harbin, China, in 2014 and 2017, respectively. His major research fields include high voltage testing technology and insulation structure design.

CHAOHAI ZHANG was born in Nanjing, China. He received the B.S. degree from the Harbin Institute of Technology (HIT), the M.S. degree from the Navy Aeronautical Engineering Academy (NAEA), and the Ph.D. degree from The Hong Kong Polytechnic University (HKPU). After 16 years' experience of research working as a JSPS Research Fellow in Japan and as a Research Engineer in Canada, respectively, he is currently a Professor with the School of Electrical Engineering and Automation, Harbin Institute of Technology. His research interests are in electrical discharges, plasma, electrical environment and condition monitoring, and diagnosis of electric power equipment.